

Magnetodielectric effect in the $S = 1/2$ quasi-two dimensional antiferromagnet $K_2V_3O_8$

R. C. Rai,¹ J. Cao,¹ J. L. Musfeldt,¹ D. J. Singh,² X. Wei,³ R. Jin,² Z. X. Zhou,² B. C. Sales,² and D. Mandrus²

¹*Department of Chemistry, University of Tennessee, Knoxville, TN 37996*

²*Oak Ridge National Laboratory, P. O. Box 2008, Oak Ridge, Tennessee 37831*

³*National High Magnetic Field Laboratory, Florida State University, Tallahassee, Florida 32310*

We report the optical and magneto-optical properties of $K_2V_3O_8$, an $S=1/2$ quasi-two-dimensional Heisenberg antiferromagnet. Local spin density approximation electronic structure calculations are used to assign the observed excitations and analyze the field dependent features. Two large magneto-optical effects, centered at ~ 1.19 and 2.5 eV, are attributed to field-induced changes in the $V^{4+} d \rightarrow d$ on-site excitations due to modification of the local crystal field environment of the VO_5 square pyramids with applied magnetic field. Taken together, the evidence for a soft lattice, the presence of vibrational fine structure on the sharp 1.19 eV magneto-optical feature, and the fact that these optical excitations are due to transitions from a nearly pure spin polarized $V d$ state to hybridized states involving both V and O , suggest that the magneto-dielectric effect in $K_2V_3O_8$ is driven by strong lattice coupling.

PACS numbers: 78.20.-e, 78.20.Ls, 71.20.-b, 75.50.Ee

I. INTRODUCTION

Thermochromic, electrochromic, piezochromic, and photochromic materials have attracted a great deal of attention in recent years^{1,2,3,4,5,6,7,8} due to the compelling underlying physics as well as possible device applications. As a simple example of physical tuning, HgI_2 changes color (from red to yellow) with temperature due to an α - to β -phase structural transition.⁹ At least one $Cu_2(\text{radical-ligand})_2$ complex shows thermochromism, changing from brown-black to green with decreasing temperature.¹⁰ Electrochromic effects have been observed in a number of conjugated polymers¹¹ and density wave materials,¹² effects attributed to doping/dedoping and polarization modifications. An applied electric field can also provide reversible modulation of the magnetic moment and coercive field, as demonstrated in Co-doped anatase TiO_2 -based devices,¹³ and magnetic phase control, as illustrated by recent work on $HoMnO_3$.¹⁴ Hydrostatic pressure and shear stress can change bond distances and angles, modifying the crystal field environment around a transition metal site. For instance, with increasing pressure, $Pt(\text{diphenylglyoximate})_2$ turns from red-brown to green above 0.4 GPa; upon rotation of the anvil, the green film turns yellow.^{15,16} In the area of photochromism, a photoinduced insulator-to-metal transition has been observed in the low-bandwidth magnetite $Pr_{0.7}Ca_{0.3}MnO_3$,¹⁷ and photoinduced reflectance changes combined with charge order domain switching have been discovered in $Bi_{0.3}Ca_{0.7}MnO_3$.¹⁸

An applied magnetic field can also induce dielectric property changes. Low frequency magneto-dielectric effects have been reported in garnet, $HoMnO_3$, $DyMnO_3$, and $DyMn_2O_5$ due to cross-coupling effects.^{19,20,21,22,23} Ferromagnetic $SeCuO_3$ displays a giant magneto-dielectric and magneto-capacitance response due to coupling of magnetic fluctuations to optical phonons.²⁴

Strong coupling between magnetism and dielectric property is also observed in La_2NiMnO_6 .²⁵ Higher frequency dielectric changes are also of interest. With a handful of recent reports on magnetic field-induced color changes in low-dimensional materials such as $Li_{0.9}Mo_6O_{17}$, $(CPA)_2CuBr_4$, and $(La_{0.4}Pr_{0.6})_{1.2}Sr_{1.8}Mn_2O_7$,^{26,27,28} it is clearly useful to elucidate the operative mechanisms, increase the size of the magneto-dielectric effect, and assert molecular-level control over the important coupling processes. $K_2V_3O_8$ offers an opportunity to explore how structural and electronic degrees of freedom can be coupled in layered, inhomogeneously mixed-valent systems. Photo-induced magnetism, observed for instance in Prussian blue and related derivatives,^{29,30,31,32,33,34,35} $Mn(\text{TCNE})_x \cdot y(\text{CH}_2\text{Cl}_2)$ and $V(\text{TCNE})_2$ molecular magnets,^{36,37} and dilute magnetic alloy semiconductors such as $(Ga, Mn)As$ thin films³⁸ complements on-going work on magneto-dielectric effects. It is also of interest to manipulate ferromagnetism with light in the junction geometry³⁹ and to combine

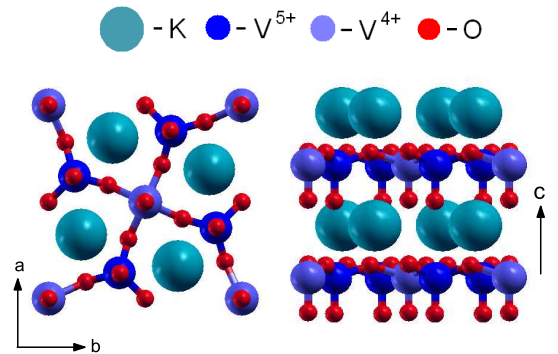


FIG. 1: (Color online) Two views of the $K_2V_3O_8$ crystal structure. View along c -axis (Left) and view along b -axis (Right).

properties as in the multiferroic systems.^{40,41}

Figure 1 displays the tetragonal crystal structure of $\text{K}_2\text{V}_3\text{O}_8$.⁴² It consists of layers of corner-sharing VO_5 square pyramids with magnetic V^{4+} ($S = 1/2$) ions and VO_4 tetrahedra with nonmagnetic V^{5+} ($S = 0$) ions, separated by interstitial K^+ ions. $\text{K}_2\text{V}_3\text{O}_8$ displays a structural phase transition at ~ 110 K, driven by a distortion of the apical oxygen of the VO_5 square pyramids and a distortion of the unit cell along the b direction.^{43,44,45} A weaker basal plane distortion was also observed near 60 K.⁴³ From the magnetic properties point of view, $\text{K}_2\text{V}_3\text{O}_8$ is an $S = 1/2$ two-dimensional Heisenberg antiferromagnet, with exchange constant $J = 12.6$ K. It undergoes Néel ordering at $T_N = 4$ K, exhibits unusual field-induced spin reorientations (spin-flop for $H\parallel c$ and spin-rotation for $H\perp c$) due to the interplay between Dzyaloshinskii-Moriya interactions and easy axis anisotropy,⁴⁶ and displays dramatic field-induced enhancement of thermal conductivity below 6 K.⁴⁵ The broad peak in the susceptibility^{46,47} near 15 K is considered to be a classic signature of two-dimensional short-range spin correlations in the ab -plane.^{48,49} Recent theoretical work suggests a scenario where the Dzyaloshinskii-Moriya interaction suppresses quantum fluctuations and yields an out-of-plane spin canting angle of the form $\cos(\theta) = H/H_S$, where $H_S = 4S(1 + \sqrt{1 + D^2})$ is the saturation field.⁵⁰ For applied field in the ab plane, one of the magnon branches is predicted to have an unusual dependence on the Dzyaloshinskii-Moriya coupling that changes with the size of the field, giving rise to a possible non-analytic behavior of the spin gap.⁵⁰

In order to investigate the interplay between spin, lattice, and charge degrees of freedom in low-dimensional, inhomogeneously mixed-valent vanadates, we measured the optical and magneto-optical properties of $\text{K}_2\text{V}_3\text{O}_8$. We observed two prominent magneto-dielectric effects at base temperature that derive from the field-induced changes in the local crystal field environment around the VO_5 square pyramid. Combined with evidence for a soft lattice, the presence of vibrational fine structure on the 1.19 eV magneto-optical feature, and the fact that these optical excitations are due to transitions from a nearly pure spin polarized $\text{V } d$ state to hybridized states involving both V and O suggest that the magneto-dielectric effects in $\text{K}_2\text{V}_3\text{O}_8$ may be driven by strong lattice coupling.

II. METHODS

A. Crystal Growth and Magnetic Characterization

Single crystals of $\text{K}_2\text{V}_3\text{O}_8$ were grown by cooling appropriate amounts of VO_2 in a molten KVO_3 flux in a platinum crucible.⁵¹ Typical crystal dimensions are $\approx 5 \times 5 \times 1$ mm³. Smooth sample surfaces were prepared by cleaving the crystals parallel to the ab -plane and cleaning with warm water.

High field magnetization studies were carried out using a vibrating sample magnetometry technique for $H\parallel c$ and $H\parallel ab$. The experiments were performed between 1.6 and 20 K using a 33 T resistive magnet at the National High Magnetic Field Laboratory (NHMFL) in Tallahassee, FL.

B. Spectroscopic Investigations

Near normal ab -plane reflectance of $\text{K}_2\text{V}_3\text{O}_8$ was measured over a wide energy range (3.7 meV - 6.5 eV) using several different spectrometers including a Bruker 113 V Fourier transform infrared spectrometer, a Bruker Equinox 55 Fourier transform infrared spectrometer equipped with an infrared microscope, and a Perkin Elmer Lambda 900 grating spectrometer, as described previously.⁵² The spectral resolution was 2 cm^{-1} in the far and middle-infrared and 2 nm in the near-infrared, visible, and near-ultraviolet. Optical conductivity was calculated by a Kramers-Kronig analysis of the measured reflectance.⁵³ An open flow cryostat and temperature controller provided temperature control.

The magneto-optical properties of $\text{K}_2\text{V}_3\text{O}_8$ were investigated between 0.8 and 3.5 eV using a grating spectrometer equipped with InGaAs and CCD detectors and a 33 T resistive magnet at the NHMFL. 150 and 600 lines/mm gratings were used, as appropriate. Experiments were performed between 2.5 and 30 K for $H\parallel c$. The field-induced changes in the measured reflectance were studied by taking the ratio of reflectance at each field and reflectance at zero field, i.e., $[R(H)/R(H = 0 \text{ T})]$. This normalized response is a sensitive way to view the field-induced optical changes.⁵⁴ To obtain the 30 T optical conductivity, we renormalized the zero-field absolute reflectance with the high-field reflectance ratios, and recalculated σ_1 using Kramers-Kronig techniques.⁵³

C. Electronic Structure Calculations

First principles, local spin density approximation (LSDA) calculations were done in order to better understand the electronic, magnetic and optical properties of $\text{K}_2\text{V}_3\text{O}_8$. These were performed using the general potential linearized augmented planewave (LAPW) method and with the augmented planewave plus local orbital modification using well converged basis sets.^{55,56,57,58} Local orbital extensions were employed to include the high lying semi-core states as well as to relax any linearization errors.⁵⁹ The calculations included no shape approximations to either the potential or charge density. Relativity was included for the valence states within a scalar relativistic approximation, while full relativity was included for the core states, within an atomic-like approximation.

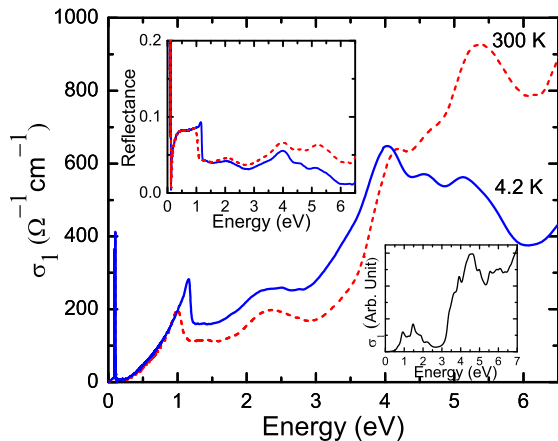


FIG. 2: (Color online) The *ab*-plane optical conductivity spectra of $K_2V_3O_8$, extracted from the measured reflectance (upper inset) by a Kramers-Kronig analysis. The lower inset shows the calculated optical conductivity, obtained from an analysis of the electronic structure, with 0.1 eV Lorentzian broadening.

III. RESULTS AND DISCUSSION

A. Understanding the Electronic Structure of $K_2V_3O_8$

Figure 2 displays the *ab*-plane optical conductivity of $K_2V_3O_8$. The spectra show strong electronic and vibrational excitations, characteristic of a semiconductor with an 0.5 eV optical gap. Based on our electronic structure calculations (discussed in detail below) and comparison with chemically similar model compounds,^{60,61,62,63,64} we assign the features centered at ~ 1 and 2.3 eV to nearly spin-polarized $V^{4+} d \rightarrow d$ on-site excitations in the majority spin channel. The 1 eV feature blueshifts with decreasing temperature and is sensitive to the 110 K structural phase transition.⁴³ We also assign the ~ 4.0 , 4.6, and 5.2 eV features in the low temperature optical conductivity spectrum as $O 2p \rightarrow V 3d$ charge transfer excitations. These features display strong temperature dependence. Partial sum rule calculations (not shown) indicate that oscillator strength is conserved up to 5.5 eV, above which the 300 K response is slightly larger.

We assigned the observed excitations in the optical conductivity (Fig. 2) based upon our electronic structure investigations. The experimental non-centrosymmetric tetragonal crystal structure (spacegroup $P4bm$, with two formula units per cell, Fig. 1) measured at 120 K was used in these calculations. This crystal structure has two different V sites, V1 (one per formula unit) and V2 (two per formula unit). The V1 atoms are closely coordinated by apical O atoms (denoted O1) at a distance of 2.94 Bohr, forming vanadyl ions. Neutron scattering experiments show V spins associated with the V1 sites, which at low temperature order antiferromagnetically in a simple alternating nearest neighbor pattern within the 2D V-

O sheets.⁴⁶ This is the same ground state that is found in the LSDA. Spin polarized calculations yield local spin moments of $1 \mu_B$ associated with the V1 sites (the insulating ferromagnetic configuration has a spin moment of exactly $1 \mu_B$ /V1 site; the antiferromagnetic ground state has the same moment inside the V1 LAPW spheres as the ferromagnetic case to within $0.002 \mu_B$). The V2 sites are found to be in a d^0 configuration with no moment as expected. The energy for the antiferromagnetic configuration is 0.22 eV per formula unit below that of a constrained non-spin-polarized calculation, reflecting the Hund's coupling on the vanadyl V1-O1 ions. The ferromagnetic ordered state is 0.055 eV per formula unit higher than the lowest energy antiferromagnetic state. Both magnetically ordered states display insulating gaps. Thus strong local moment character is found. The magnetic exchange energy corresponding to the difference in energy of the antiferromagnetic and ferromagnetic states may be an overestimate due to an overestimation of hopping integrals in the LSDA. However, even taking this into account, it is very large considering the low experimental T_N . Assuming that the lattice distortion associated with the 110 or 60 K transitions does not substantially decrease the exchange coupling, this indicates a substantial reduction of the ordering temperature due to the strong two dimensionality of the compound. Thus, especially in-plane, though fluctuating, the V1 moments should be locally antiferromagnetic at temperatures considerably above T_N . This is consistent with the experimental observation of a susceptibility maximum at ~ 15 K.^{46,47}

The band structure for the antiferromagnetic ground state is shown in Fig. 3. Projections of the density of states onto the V and the O1 (apical O above V1) LAPW spheres are shown in Fig. 4. The electronic structure shows a main gap of 3.5 eV, which separates a manifold of occupied O $2p$ derived bands from an unoccupied conduction band manifold, which derived from V $3d$ states near the bottom. There are two bands in the gap. These are the exchange split vanadyl majority and minority spin states. These are very flat bands, and show practically

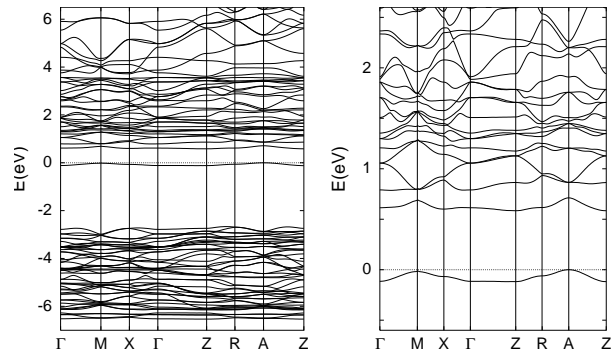


FIG. 3: LSDA band structure (left) and blow up (right) for antiferromagnetic $K_2V_3O_8$. The energy zero is the highest occupied state.

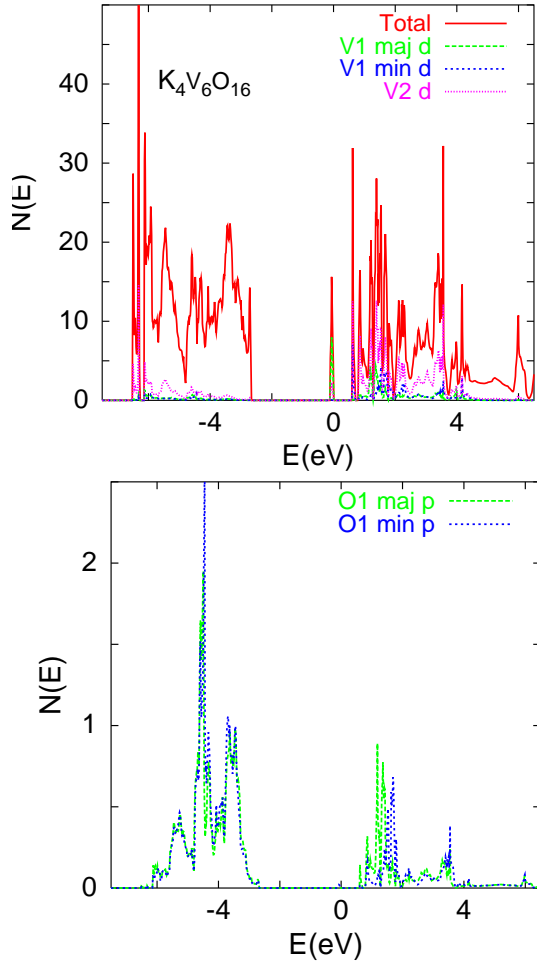


FIG. 4: (Color online) Projections of the electronic density of states onto the various atomic sites, as measured by projections onto the corresponding LAPW spheres. The sphere radii are 1.68 Bohr and 1.35 Bohr for V (top) and O (bottom), respectively.

the same dispersion, reflecting the weak interaction of these split off states with the other orbitals. The LSDA exchange splitting of the vanadyl magnetic d state is 0.73 eV. The band gap is smaller (0.58 eV) due to the ~ 0.15 eV width of these bands. However, optical transitions at this energy would be forbidden both because of the indirect nature of the gap, and more importantly because this is a spin-flip transition. The lowest allowed transitions would be from the majority spin vanadyl state to the edge of the main conduction manifold, starting at 0.90 eV. Since the unoccupied, minority spin vanadyl state lies 3.4 eV above the main O 2p band edge, all optical transitions up to 3.4 eV are from the polarized majority vanadyl 3d state to the conduction bands, and are in the majority spin channel only. As may be seen from the projections of the density of states, the occupied vanadyl state (this is the d state of the crystal field 3d shell of V in the presence of the very short V1-O1 bond), has practically pure V1 d character, as expected. However,

the higher lying Vd states have substantial hybridization with O 2p orbitals. Transitions from the main O 2p derived valence band manifold to the main conduction bands, which would be expected to yield a strong optical signal, would begin at 3.5 eV.

This picture is reflected in the calculated LSDA optical conductivity, shown in the lower inset of Fig. 2. A broad feature is found extending from ~ 0.9 to 2.0 eV, derived from two strong peaks at 0.9 eV and 1.5 eV, plus three smaller peaks, with a strong edge beginning at ~ 3.5 eV, and a prominent peaks at 4.0 and 4.6 eV. While the agreement with experiment is by no means perfect, the comparison does allow identification of the main features. In particular, the features can be mapped onto the experiment by noting that the main peaks are shifted consistent with a downward shift of the majority occupied d level in the experiment by approximately 0.5 eV, relative to the LSDA band structure, perhaps due to Mott-Hubbard correlations. Allowing for such a shift, the LSDA optical conductivity is more similar to the 300 K data than the 4 K data, which presumably reflects the effect of the structural transition at 110 K. In any case, the comparison allows us to identify the magnetochromic features in the optical spectrum as deriving from transitions in the majority spin only between the occupied V1 d state and hybridized V-O conduction band states. One test of this basic picture of the electronic structure would be to measure the transport gap, which should be smaller than the optical gap in the scenario above.

B. Magneto-Dielectric Properties of $K_2V_3O_8$

Figure 5 displays a close-up view of the magneto-optical response of $K_2V_3O_8$, $R(H)/R(0\text{ T})$ for $H||c$, at 4.2 K.⁶⁵ The applied magnetic field decreases the overall reflectance in a significant and systematic way in both the near infrared (at ~ 1.19 eV) and in the optical regime (centered at ~ 2.5 eV). The feature centered at 1.19 eV (Fig. 5(a)) is sharp and displays a great deal of fine structure that increases in amplitude with applied field, whereas the feature near 2.5 eV (Fig. 5(b)) is very broad. Based upon the energy scale of these magneto-optical effects, both structures are associated with field-induced changes in the V^{4+} $d \rightarrow d$ on-site excitations. We refer to this type of effect as “magnetochromism” when it occurs in the visible range.

Figure 6 shows the detailed temperature dependence of the 1.19 eV reflectance ratio feature at $H = 32$ T. Here, the overall effect increases with decreasing temperature, saturating near 4 K ($\approx T_N$). The 1.19 eV reflectance ratio structure is punctuated by several sidebands, each spaced by ~ 6.8 meV (55 cm^{-1}). This is a vibrational energy scale. Thus, these sidebands provide experimental evidence that lattice coupling may be important in $K_2V_3O_8$. Interestingly, the prominent low temperature vibrational fine structure on the 1.19 eV reflectance ratio feature disappears through the 15 K transition, which

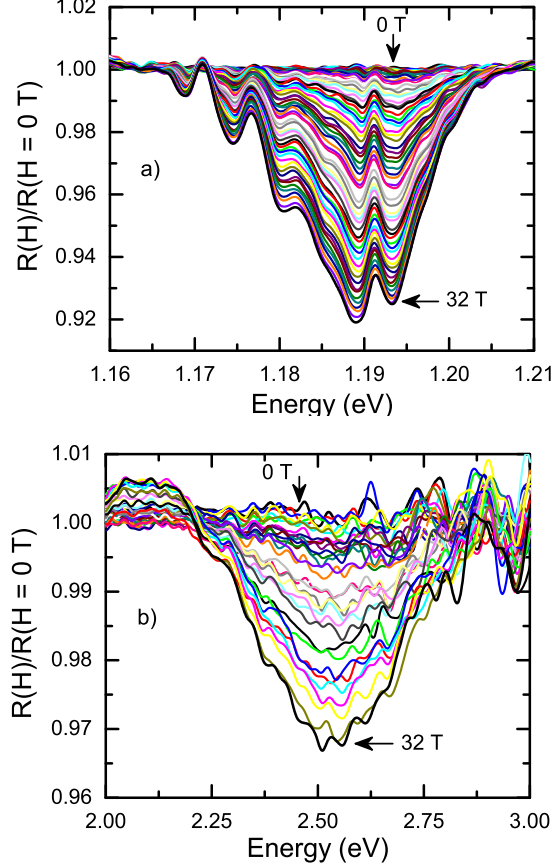


FIG. 5: (Color online) The normalized *ab*-plane magneto-optical response, $R(H)/R(0\text{ T})$, of $\text{K}_2\text{V}_3\text{O}_8$ for magnetic fields between 0 and 32 T ($H\parallel c$) at 4.2 K (a) A sharp structure centered at 1.19 eV is observed in the near infrared. Data are taken with 0.5 T steps to highlight the multiphonon coupling. (b) A broad structure centered at 2.5 eV is observed in the color band region. Data are taken with 1 T steps.

is associated with formation of magnetic correlations in this highly 2D system. Degradation of short-range spin correlations also gives rise to a peak in the thermal conductivity and magnetic susceptibility.⁴⁶

How do these trends manifest themselves in the optical properties? Since $\epsilon(\omega) = \epsilon_1(\omega) + i\epsilon_2(\omega) = \epsilon_1(\omega) + \frac{4\pi i}{\omega}\sigma_1(\omega)$, it is clear that the field-induced changes in reflectance, discussed in previous paragraphs, translate into finite frequency magneto-dielectric effects. For instance, to obtain the 30 T optical conductivity, we renormalize the zero-field absolute reflectance with the high-field reflectance ratio, and calculate σ_1 using Kramers-Kronig techniques.⁵³ The results are shown in Fig. 7.

The panels in Fig. 7 display close-up views of the optical conductivity of $\text{K}_2\text{V}_3\text{O}_8$ at 0 and 30 T. Based upon these results, we can directly attribute the observed magneto-optical response to field-induced modifications of the $V^{4+} d \rightarrow d$ excitations. The main effect of the applied field is to red-shift the trailing edge of the 1 eV excitation and to narrow the color band excitation centered at 2.3 eV. Analysis of the partial sum rule (not

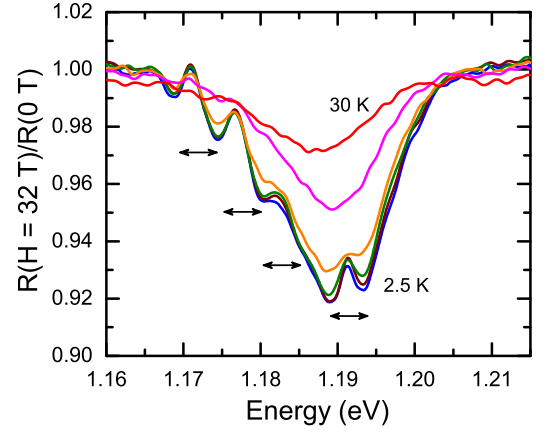


FIG. 6: (Color online) Magneto-optical response of $\text{K}_2\text{V}_3\text{O}_8$ in the *ab*-plane for $H = 32\text{ T}$ at 2.5, 4.2, 7, 10, 20, and 30 K (bottom to top). Arrows indicate the fine structures with energy scale $\sim 6.8\text{ meV}$ (55 cm^{-1}).

shown) indicates that these excitations narrow in magnetic field, perhaps due to a change in scattering rate; a very small amount of oscillator strength is missing at 30 T. One plausible origin for the modification of the $V^{4+} d \rightarrow d$ on-site excitations is a field-induced structural deformation of the VO_5 square pyramid. In this system, displacement of the vanadium ion in the square pyramids (toward the apical oxygen and out of plane) gives a very short V-O (vanadyl-type) bond. Given the evidence for a soft lattice (detailed below), distortion of the local crystal field environment in the VO_5 square pyramid may be driven by a magneto-elastic coupling mechanism. The fact that the optical transitions below 3.5 eV are due to transitions from a nearly pure spin polarized V d state to hybridized states, involving V and O states, also suggests the possibility of strong lattice coupling.

To complement our magneto-optics results, we inves-

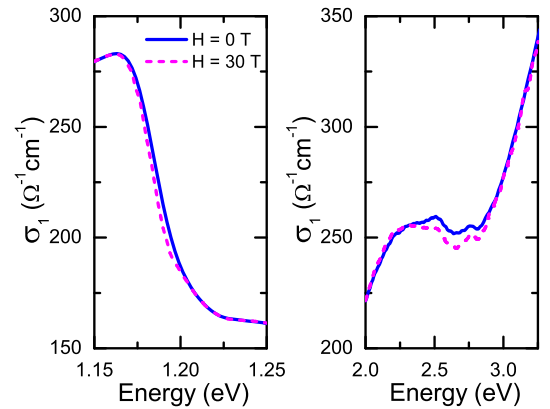


FIG. 7: (Color online) The *ab*-plane optical conductivity spectra of $\text{K}_2\text{V}_3\text{O}_8$ at $H = 0\text{ T}$ (solid line) and $H = 30\text{ T}$ (dashed line) at 4.2 K.

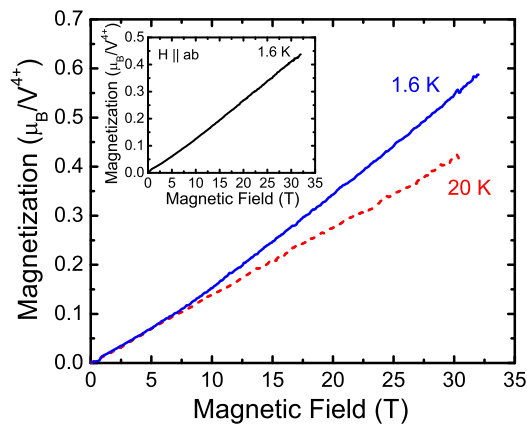


FIG. 8: (Color online) Magnetization of $\text{K}_2\text{V}_3\text{O}_8$ as a function of applied magnetic field ($H\parallel c$) at 1.6 K (solid line) and 20 K (dashed line). The inset shows the magnetization for $H\parallel ab$ at 1.6 K. On this scale, magnetization will saturate at $1 \mu_B/V^{4+}$.

tingated the high-field magnetization of $\text{K}_2\text{V}_3\text{O}_8$ (Fig. 8). At 20 K, the magnetization increases more or less linearly up to at least 33 T due to the gradual alignment of spins towards the applied field direction by tilting out of the basal plane.⁶⁶ A careful inspection of the low temperature data reveals nonlinear behavior for both $H\parallel c$ and $H\parallel ab$. As shown in Fig. 8, the slope dM/dH clearly increases above 9 T at 1.6 K, with no sign of saturation up to 33 T for both $H\parallel c$ and $H\parallel ab$. Apparently, the high magnetic field reduces the antiferromagnetic coupling strength at low temperatures. Based on the work of Chernyshev,⁵⁰ we estimate the canting angle to be $\sim 29^\circ$ at 33 T ($H\parallel c$). Besides the change in slope at 9 T, there are no other features in the magnetization that correlate with the optical properties.

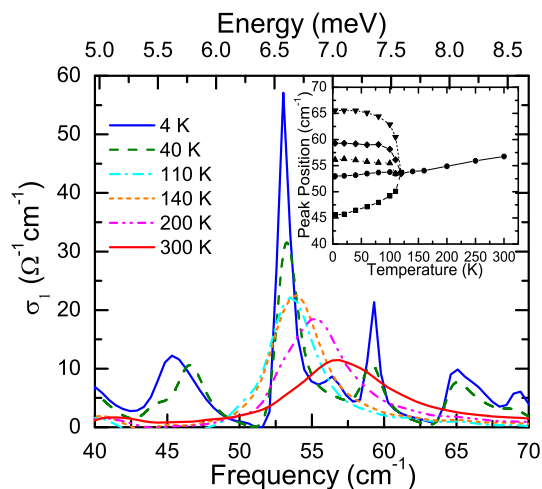


FIG. 9: (Color online) Peak splitting in the far infrared spectra of $\text{K}_2\text{V}_3\text{O}_8$ at different temperatures. The inset shows the center frequency of the 55 cm^{-1} vibrational mode versus temperature.

In order to further elucidate the role of the lattice in mediating the magneto-dielectric response, we measured the variable temperature vibrational properties of $\text{K}_2\text{V}_3\text{O}_8$. Several modes show softening and splitting at low temperature, evidence of the 110 K structural distortion and a soft lattice. Based on vibrational properties studies in similar vanadyl oxide compounds,^{67,68,69,70,71} the features of interest below 500 cm^{-1} can be assigned as V-O-V bending, O-V-O bending, and other low-energy torsional and twisting motions of the square pyramidal and tetrahedral building block units. The behavior of the 6.8 meV (55 cm^{-1}) cluster (Fig. 9) is typical of the low temperature mode splitting in $\text{K}_2\text{V}_3\text{O}_8$. Similar splitting is observed near 17.4 meV (140 cm^{-1}) (doublet), 45.3 meV (365 cm^{-1}) (quintuplet), and 52.9 meV (427 cm^{-1}) (doublet). Interestingly, the energy scale of the 6.8 meV (55 cm^{-1}) mode matches that of the multiphonon fine structure observed at 1.19 eV in the magneto-optical response (Fig. 5(a)). To check for direct evidence of magneto-elastic interactions, we carried out independent magneto-infrared measurements of $\text{K}_2\text{V}_3\text{O}_8$. There is no magnetic field dependence of the 6.8 meV mode up to 17 T, within our sensitivity. That said, it is important to note that $\text{K}_2\text{V}_3\text{O}_8$ has many infrared, Raman, and inactive vibrational modes. Raman-active torsional modes that flex the VO_5 square pyramids out of the plane at this energy scale would seem to be likely candidates for coupling to the magnetic system. We carried out LSDA calculations of some of the zone center phonons, and find modes of this character in the appropriate frequency range. $\text{SrCu}_2(\text{BO}_3)_2$ also has similar Raman-active out-of-plane motions of almost all ions that couple to the magnetic system.⁷² The coupling of a soft phonon mode (or other lattice degrees of freedom) with localized spins is responsible for magneto-dielectric effects in antiferromagnets such as EuTiO_3 , DyMn_2O_5 , and HoMnO_3 as well.^{20,23,73} Future work will focus on the connection between high and low frequency magneto-dielectric effects in $\text{K}_2\text{V}_3\text{O}_8$ and other materials.

IV. CONCLUSION

We investigated the optical, magneto-optical, and LSDA electronic structure properties of $\text{K}_2\text{V}_3\text{O}_8$, a model $S=1/2$ quasi-two-dimensional Heisenberg antiferromagnet. The spectral response is similar to that of other inhomogeneously mixed-valent vanadates, with a 0.5 eV semiconducting gap and both $V^{4+} d \rightarrow d$ on-site and $\text{O } 2p \rightarrow \text{V } 3d$ charge transfer excitations. According to our electronic structure calculations, the on-site $d \rightarrow d$ transitions emanate from strongly spin polarized (majority channel) excitations. Application of magnetic field modifies the optical properties in two regimes: (1) on the trailing edge of the 1 eV excitation and (2) in the shape of the color band near 2.5 eV . These effects are attributed to changes in the $V^{4+} d \rightarrow d$ on-site excitations due to field-induced local distortion of the VO_5 square

pyramid. Combined with evidence for a soft lattice, the presence of vibrational fine structure on the sharp 1.19 eV magneto-optical feature, and the fact that these optical excitations are due to transitions from a nearly pure spin polarized $V d$ state to hybridized states involving both V and O suggest that the magneto-dielectric effect in $K_2V_3O_8$ may be driven by strong lattice coupling. We discussed the type of low-energy vibrational modes that might couple the VO_5 square pyramids to the magnetic system.

V. ACKNOWLEDGMENTS

Work at the University of Tennessee is supported by the Materials Science Division, Basic Energy Sciences,

U.S. Department of Energy (DE-FG02-01ER45885). Oak Ridge National Laboratory is managed by UT-Battelle, LLC, for the U.S. Dept. of Energy under contract DE-AC05-00OR22725. A portion of this work was performed at the NHMFL, which is supported by NSF Cooperation Agreement DMR-0084173 and by the State of Florida. We thank Igor I. Mazin for interesting discussions and Sonal Brown for technical assistance.

-
- ¹ J. Casado, R. P. Ortiz, J. T. L. Navarrete, S. Ito, and N. Morita, *J. Phys. Chem.* **108**, 18463 (2004).
 - ² D. M. DeLongchamp and P. T. Hammond, *Chem. Mater.* **16**, 4799 (2004).
 - ³ S. Hayashi, K. Asada, S. Horiike, H. Furuhashi, and T. Hirai, *J. Coll. Int. Sci.* **176**, 370 (1995).
 - ⁴ M. S. R. Khan, K. A. Khan, W. Estrada, and C. G. Granqvist, *J. Appl. Phys.* **69**, 3231 (1991).
 - ⁵ P. Koidl, K. W. Blazey, W. Berlinger, and K. A. Müller, *Phys. Rev. B* **14**, 2703 (1976).
 - ⁶ R. L. Wild, E. M. Rockar, and J. C. Smith, *Phys. Rev. B* **8**, 3828 (1973).
 - ⁷ F. Rodriguez, D. Hernandez, J. Garcia-Jaca, H. Ehrenberg, and H. Weitzel, *Phys. Rev. B* **61**, 16 497 (2000).
 - ⁸ B. W. Faughnan, *Phys. Rev. B* **4**, 3623 (1971).
 - ⁹ J. W. Hill, R. H. Petrucci, T. W. McCreary, and S. S. Perry, *General Chemistry* (Pearson Prentice Hall, New Jersey, 2005).
 - ¹⁰ P. M. Lahti, unpublished results.
 - ¹¹ A. A. Argun, P. Aubert, B. C. Thompson, I. Schwendeman, C. L. Gaupp, J. Hwang, N. J. Pinto, D. B. Tanner, A. G. MacDiarmid, and J. R. Reynolds, *Chem. Mater.* **16**, 4401 (2004).
 - ¹² M. E. Itkis and J. W. Brill, *Phys. Rev. Lett.* **72**, 2049 (1994).
 - ¹³ T. Zhao, S. R. Shinde, S. B. Ogale, H. Zheng, T. Venkatesan, R. Ramesh, and S. Das Sarma, *Phys. Rev. Lett.* **94**, 126601 (2005).
 - ¹⁴ T. Lottermoser, T. Lonkai, U. Amann D. Hohlwein, J. Ihlinger, and M. Fiebig, *Nature* **430**, 541 (2004).
 - ¹⁵ M. Inokuchi, A. Nagaoka, M. Yamamoto, I. Shirotnani, J. Hayashi, K. Yakushi, H. Kawamura, and H. Inokuchi, *Synthetic Metals* **152**, 421 (2005).
 - ¹⁶ I. Shirotnani, J. Hayashi, K. Hirano, H. Kawamura, M. Inokuchi, K. Yakushi, and H. Inokuchi, *Proc. Japan Acad.* **79**, Ser. B 267 (2003).
 - ¹⁷ K. Miyano, T. Tanaka, Y. Tomioka, and Y. Tokura, *Phys. Rev. Lett.* **78**, 4257 (1997).
 - ¹⁸ I. I. Smolyaninov, V. N. Smolyaninova, C. C. Davis, B. -G. Kim, S. -W. Cheong, and R. L. Greene, *Phys. Rev. Lett.* **87**, 127204 (2001).
 - ¹⁹ N. Hur, S. Park, S. Guha, A. Borissov, V. Kiryukhin, and S. -W. Cheong, *Appl. Phys. Lett.* **87**, 042901 (2005).
 - ²⁰ C. de la Cruz, F. Yen, B. Lorenz, Y. Q. Wang, Y. Y. Sun, M. M. Gospodinov, and C. W. Chu, *Phys. Rev. B* **71**, 060407(R) (2005).
 - ²¹ B. Lorenz, A. P. Litvinchuk, M. M. Gospodinov, and C. W. Chu, *Phys. Rev. Lett.* **92**, 087204 (2004).
 - ²² T. Goto, T. Kimura, G. Lawes, A. P. Ramirez, and Y. Tokura, *Phys. Rev. Lett.* **92**, 257201 (2004).
 - ²³ N. Hur, S. Park, P. A. Sharma, S. Guha, and S-W Cheong, *Phys. Rev. Lett.* **93**, 107207 (2004).
 - ²⁴ G. Lawes, A. P. Ramirez, C. M. Varma, and M. A. Subramanian, *Phys. Rev. Lett.* **91**, 257208 (2003).
 - ²⁵ N. S. Rogado, J. Li, A. W. Sleight, and M. A. Subramanian, *Adv. Mater.* **17**, 2225 (2005).
 - ²⁶ J. Choi, J. D. Woodward, J. L. Musfeldt, X. Wei, M. H. Whangbo, J. He, R. Jin, and D. Mandrus, *Phys. Rev. B* **70**, 085107 (2004).
 - ²⁷ J. Choi, J. D. Woodward, J. L. Musfeldt, J. T. Haraldsen, X. Wei, M. Apostu, R. Suryanarayanan, and A. Revcolevschi, *Phys. Rev. B* **70**, 064425 (2004).
 - ²⁸ J. D. Woodward, J. Choi, J. L. Musfeldt, J. T. Haraldsen, X. Wei, H. -J. Koo, D. Dai, M. -H. Whangbo, C. P. Landee, and M. M. Turnbull, *Phys. Rev. B* **71**, 174416 (2005).
 - ²⁹ O. Sato, T. Iyoda, and A. Fujishima, *Science* **272**, 704 (1996).
 - ³⁰ T. Kawamoto, Y. Asai, and S. Abe, *Phys. Rev. B* **60**, 12990 (1999).
 - ³¹ M. Verdaguer, A. Bleuzen, C. Train, R. Garde, F. F. de Biani, and C. Desplanches, *Phil. Trans. R. Soc. London A*, **357**, 2959 (1999).
 - ³² J. G. Moore, E. J. Lochner, C. Ramsey, N. S. Dalal, and A. E. Stiegman, *Angew. Chem.* **42**, 2741 (2003).
 - ³³ D. A. Pejarković, J. L. Manson, J. S. Miller, and A. J. Epstein, *Phys. Rev. Lett.* **85**, 1994 (2000).
 - ³⁴ C. P. Berlinguette, A. Dragulescu-Andrasi, A. Sieber, J. R. Galán-Mascarós, H. Güdel, C. Achim, and K. R. Dunbar, *J. Am. Chem. Soc.* **126**, 6222 (2004).
 - ³⁵ J. S. Miller, *MRS Bulletin* **25**, 60 (Nov. 2000).
 - ³⁶ D. A. Pejarković, C. Kitamura, J. S. Miller, and A. J. Epstein, *Phys. Rev. Lett.* **88**, 057202 (2002).
 - ³⁷ M. A. Girtu, C. M. Wynn, J. Zhang, J. S. Miller, and A. J. Epstein, *Phys. Rev. B* **61**, 492 (2000).

- ³⁸ A. Oiwa, Y. Mitsumori, R. Moriya, T. Slupinski, and H. Munekata, *Phys. Rev. Lett.* **88**, 137202 (2002).
- ³⁹ I. Žutić, J. Fabian, S. Das Sarma, *Rev. Mod. Phys.* **76**, 323 (2004).
- ⁴⁰ T. Kimura, T. Goto, H. Shintani, K. Ishizaka, T. Arima, and Y. Tokura, *Nature* **426**, 55 (2003).
- ⁴¹ B. B. Van Aken, T. T. M. Palstra, A. Filippetti, and N. A. Spaldin, *Nature Materials* **3**, 164 (2004).
- ⁴² P. J. Galy and A. Carpy, *Acta Cryst.* **B31**, 1974 (1975).
- ⁴³ J. Choi, Z. T. Zhu, J. L. Musfeldt, G. Ragghianti, D. Mandrus, B. C. Sales, and J. R. Thompson, *Phys. Rev. B* **65**, 054101 (2001).
- ⁴⁴ R. L. Withers, T. Höche, Y. Liu, S. Esmaeilzadeh, R. Keding, and B. Sales, *J. Solid State Chem.* **177**, 3316 (2004).
- ⁴⁵ B. C. Sales, M. D. Lumsden, S. E. Nagler, D. Mandrus, and R. Jin, *Phys. Rev. Lett.* **88**, 095901 (2002).
- ⁴⁶ M. D. Lumsden, B. C. Sales, D. Mandrus, S. E. Nagler, and J. R. Thompson, *Phys. Rev. Lett.* **86**, 159 (2001).
- ⁴⁷ G. Liu and J. E. Greedan, *J. Solid State Chem.* **114**, 499 (1995).
- ⁴⁸ V. Hardy, M. R. Lees, A. Maignan, S. Hébert, D. Flahaut, C. Martin, and D. McK Paul, *J. Phys.: Condens. Matter* **15** 5737 (2003).
- ⁴⁹ E. M. L. Chung, M. R. Lees, G. J. McIntyre, C. Wilkinson, G. Balakrishnan, J. P. Hague, D. Visser, and D. McK Paul, *J. Phys.: Condens. Matter* **16**, 7837 (2004).
- ⁵⁰ A. L. Chernyshev, *Phys. Rev. B* **72**, 174414 (2005).
- ⁵¹ About 100 grams of V_2O_5 (99.995 %) and 76 grams of K_2CO_3 (99.997%) is loaded into a 250 ml Pt crucible and slowly heated in air to 700 °C and held for 2 hours. The powder is added in two stages because of substantial foaming. The molten KVO_3 flux is cooled to room temperature and the Pt crucible and solidified KVO_3 is loaded into a fused silica ampoule that is necked down at the top. Using a long funnel, 9 grams of VO_2 (99 %) is added to the Pt crucible and the entire ampoule is evacuated and sealed. The sealed ampoule is loaded into a furnace and heated to 850 °C for 6 hours, cooled to 700 °C over 1h and then cooled to about 400 °C at 1 °C/h, followed by furnace cooling to room temperature. The KVO_3 flux is removed with a combination of warm water and ultrasonic vibration. The resulting $K_2V_3O_8$ crystals are black rectangular plates with typical dimensions of 5 x 5 x 1 mm³.
- ⁵² Z. -T. Zhu, J. L. Musfeldt, Z. S. Teweldemedhin, and M. Greenblatt, *Phys. Rev. B* **65**, 214519 (2002).
- ⁵³ F. Wooten, *Optical Properties of Solids* (Academic Press, New York, 1972).
- ⁵⁴ A. B. Sushkov, J. L. Musfeldt, X. Wei, S. A. Crooker, J. Jegoudez, and A. Revcolevschi, *Phys. Rev. B* **66**, 054439 (2002).
- ⁵⁵ D. J. Singh, *Planewaves, Pseudopotentials and the LAPW Method* (Kluwer Academic, Boston, 1994).
- ⁵⁶ E. Sjöstedt, L. Nordstrom, and D. J. Singh, *Solid State Comm.* **114**, 15 (2000).
- ⁵⁷ Calculations were done with two different LAPW codes, an in-house LAPW code, and the WIEN2K code. These were cross-checked and found to yield the same properties.
- ⁵⁸ P. Blaha, K. Schwarz, G. K. H. Madsen, D. Kvasnicka, and J. Luitz, *WIEN2K* (Technical University of Vienna, Vienna, 2002).
- ⁵⁹ D. J. Singh, *Phys. Rev. B* **43**, 6388 (1991).
- ⁶⁰ S. Shin, S. Suga, M. Taniguchi, M. Fujisawa, H. Kanzaki, A. Fujimori, H. Daimon, Y. Ueda, K. Kosuge, and S. Kachi, *Phys. Rev. B* **41**, 4993 (1990).
- ⁶¹ K. Kobayashi, T. Mizokawa, A. Fujimori, M. Isobe, and Y. Ueda, *Phys. Rev. Lett.* **80**, 3121 (1998).
- ⁶² C. Presura, D. van der Marel, M. Dischner, C. Geibel, and R. K. Kremer, *Phys. Rev. B* **62**, 16522 (2000).
- ⁶³ K. Morikawa, T. Mizokawa, K. Kobayashi, A. Fujimori, H. Eisaki, S. Uchida, F. Iga, and Y. Nishihara, *Phys. Rev. B* **52**, 13711 (1995).
- ⁶⁴ A. A. Tsvetkov, F. P. Mena, P. H. M. van Loosdrecht, D. van der Marel, Y. Ren, A. A. Nugroho, A. A. Menovsky, I. S. Elfimov, and G. A. Sawatzky, *Phys. Rev. B* **69**, 075110 (2004).
- ⁶⁵ The magneto-optical effects discussed here are reproducible on the same crystal and crystals of different batches. There is no hysteresis in the magneto-optical response, which implies that the field-induced structural deformations are reversible.
- ⁶⁶ Two transitions were observed at ~ 0.85 T for $H\parallel c$ and at ~ 0.65 T for $H\parallel ab$, both transitions correspond to the reorientation of the V^{4+} spins, perpendicular to \mathbf{H} [consistent with Ref. 46]. Above the transition field, in both cases, spins gradually align towards the increasing field direction, resulting a linear magnetization with the applied field.
- ⁶⁷ Z. V. Popović, R. Gajić, M. J. Konstantinović, R. Provoost, V. V. Moshchalkov, A. N. Vasil'ev, M. Isobe, and Y. Ueda, *Phys. Rev. B* **61**, 11454 (2000).
- ⁶⁸ Z. V. Popović, M. J. Konstantinović, R. Gajić, V. N. Popov, M. Isobe, Y. Ueda, and V. V. Moshchalkov, *Phys. Rev. B* **65**, 184303 (2002).
- ⁶⁹ M. J. Konstantinović, Z. V. Popović, M. Isobe, and Y. Ueda, *Phys. Rev. B* **61**, 15185 (2000).
- ⁷⁰ M. J. Konstantinović, Z. V. Popović, V. V. Moshchalkov, C. Presura, R. Gajić, M. Isobe, and Y. Ueda, *Phys. Rev. B* **65**, 245103 (2002).
- ⁷¹ J. Spitaler, E. Ya. Sherman, H. G. Evertz, and C. Ambrosch-Draxl, *Phys. Rev. B* **70**, 125107 (2004).
- ⁷² K. -Y. Choi, Yu. G. Pashkevich, K. V. Lamonova, H. Kageyama, Y. Ueda, and P. Lemmens, *Phys. Rev. B* **68**, 104418 (2003).
- ⁷³ T. Katsufuji and H. Takagi, *Phys. Rev. B* **64**, 054415 (2001).